

## The thermal stability of epitaxial GeSn layers

P. Zaumseil, Y. Hou, M. A. Schubert, N. von den Driesch, D. Stange, D. Rainko, M. Virgilio, D. Buca, and G. Capellini

Citation: [APL Materials](#) **6**, 076108 (2018); doi: 10.1063/1.5036728

View online: <https://doi.org/10.1063/1.5036728>

View Table of Contents: <http://aip.scitation.org/toc/apm/6/7>

Published by the [American Institute of Physics](#)

---

### Articles you may be interested in

[Perspective: Superhard metal borides: A look forward](#)

[APL Materials](#) **6**, 070901 (2018); 10.1063/1.5040763

[Designing CdS/Se heterojunction as high-performance self-powered UV-visible broadband photodetector](#)

[APL Materials](#) **6**, 076106 (2018); 10.1063/1.5042549

[Atomically uniform Sn-rich GeSn semiconductors with 3.0–3.5  \$\mu\text{m}\$  room-temperature optical emission](#)

[Applied Physics Letters](#) **112**, 251903 (2018); 10.1063/1.5038644

[Electrical properties of extended defects in strain relaxed GeSn](#)

[Applied Physics Letters](#) **113**, 022102 (2018); 10.1063/1.5034573

[2D hexagonal photonic crystal GeSn laser with 16% Sn content](#)

[Applied Physics Letters](#) **113**, 051104 (2018); 10.1063/1.5036739

[Research Update: Recent progress on 2D materials beyond graphene: From ripples, defects, intercalation, and valley dynamics to straintronics and power dissipation](#)

[APL Materials](#) **6**, 080701 (2018); 10.1063/1.5042598

---



**Cryogenic probe stations**

for accurate, repeatable  
material measurements

## The thermal stability of epitaxial GeSn layers

P. Zaumseil,<sup>1</sup> Y. Hou,<sup>1</sup> M. A. Schubert,<sup>1</sup> N. von den Driesch,<sup>2</sup> D. Stange,<sup>2</sup>  
 D. Rainko,<sup>2</sup> M. Virgilio,<sup>3</sup> D. Buca,<sup>2</sup> and G. Capellini<sup>1,4,a</sup>

<sup>1</sup>IHP, 15236 Frankfurt (Oder), Germany

<sup>2</sup>Peter Grünberg Institute 9 (PGI-9) and JARA-Fundamentals of Future Information Technologies (JARA-FIT), Forschungszentrum Jülich, 52425 Jülich, Germany

<sup>3</sup>Dipartimento di Fisica “E. Fermi,” Università di Pisa, Largo Pontecorvo 3, I-56127 Pisa, Italy

<sup>4</sup>Dipartimento di Scienze, Università Roma Tre, Viale G. Marconi 446, I-00146 Rome, Italy

(Received 18 April 2018; accepted 19 June 2018; published online 30 July 2018)

We report on the direct observation of lattice relaxation and Sn segregation of GeSn/Ge/Si heterostructures under annealing. We investigated strained and partially relaxed epi-layers with Sn content in the 5 at. %-12 at. % range. In relaxed samples, we observe a further strain relaxation followed by a sudden Sn segregation, resulting in the separation of a  $\beta$ -Sn phase. In pseudomorphic samples, a slower segregation process *progressively* leads to the accumulation of Sn at the surface only. The different behaviors are explained by the role of dislocations in the Sn diffusion process. The positive impact of annealing on optical emission is also discussed. © 2018 Author(s). All article content, except where otherwise noted, is licensed under a Creative Commons Attribution (CC BY) license (<http://creativecommons.org/licenses/by/4.0/>). <https://doi.org/10.1063/1.5036728>

Semiconductor heterostructures comprising GeSn alloys are more and more considered a serious candidate as active material for light emitting devices integrated into the Si-CMOS technology<sup>1</sup> after the demonstration of lasing using this material system.<sup>2-4</sup> Nonetheless, in order to move toward real-market applications, several issues still have to be addressed such as the low laser operating temperature. In particular, an increase of the Sn content in the active material beyond ~12 at. %, although leading to a “more-direct” band structure, is accompanied by a higher lasing threshold<sup>5</sup> that can be attributed to a decreased structural quality of the GeSn alloy.

The investigation of the thermal stability of GeSn is limited to few studies where different deposition methods or annealing conditions were adopted.<sup>6-9</sup> Furthermore, the strain relaxation mechanisms in GeSn remain unclear and contradictory reports can be found in the literature.<sup>10</sup> This is due to the fact that several experiments were performed adopting an interpretative framework similar to that developed for SiGe alloys, a material system for which the strain relaxation and dislocation dynamics are well understood and often aprioristically considered valid for all the group IV alloys. For example, Li *et al.*<sup>6</sup> indicate that GeSn layers pseudomorphically grown on Ge buffers undergo plastic strain relaxation by thermal treatment above 420 °C, as evidenced by the formation of a strain relieving misfit dislocation (MD) network at the GeSn/Ge interface and of threading dislocations (TD) in the GeSn layers. On the other hand, Chen *et al.*<sup>7</sup> studied the change of the surface morphology and Sn diffusion in pseudomorphic Ge<sub>0.9</sub>Sn<sub>0.10</sub> layers under annealing, not observing any plastic strain relaxation.

The reduced thermal stability for GeSn alloys is a consequence of low solid solubility of Sn in Ge. Indeed, Sn surface and volume segregation by formation of Sn-rich nanodots has been evidenced,<sup>11</sup> but the proof of  $\beta$ -Sn formation at large Sn contents, as numerical *ab initio* calculations suggested,<sup>12</sup> has not been reported yet.

Here, we study the structural evolution under thermal treatment of chemical-vapor deposition grown GeSn/Ge/Si layers using *in situ* x-ray diffraction. This technique enables us to directly measure

<sup>a</sup>Author to whom correspondence should be addressed: [capellini@ihp-microelectronics.com](mailto:capellini@ihp-microelectronics.com)

the lattice parameter and the material composition as a function of the annealing temperature  $T_A$ . In order to understand how the initial degree of elastic strain and the Sn content in the GeSn alloy influence the plastic relaxation of the epitaxial strain and the Sn segregation phenomenon, we shall compare samples that are either fully pseudomorphic or largely plastically relaxed epi-layers.

We could determine, for a range of Sn contents, a temperature window in which the GeSn epilayers can be annealed to reduce the heteroepitaxial strain and increase the lattice quality while preserving the film composition. This result ultimately enables us to improve the light emission efficiency of the material, as evidenced by the narrowing and the intensity increase of the GeSn layer optical emission spectrum in photoluminescence measurements.

The GeSn layers investigated in this study were grown by means of reduced-pressure chemical vapor deposition (RP-CVD) in an industry-compatible reactor using digermane and tin tetrachloride as precursors. To minimize lattice mismatch between GeSn and the 200 mm Si(001) wafers, growth was performed on top of 2.5  $\mu\text{m}$  thick Ge buffers, which were externally produced beforehand.<sup>13</sup> Three samples, with Sn compositions equal to 5, 9, and 12 at. % (named REL5, REL9, and REL12), respectively, were grown by adjusting the growth temperature in a range between 350 °C and 400 °C. Their thickness has been chosen large enough to result in a heteroepitaxial strain plastic relaxation, as later quantified (see Table I). Details on the growth procedure, which has previously been shown to yield high quality GeSn material,<sup>2</sup> are given elsewhere.<sup>14</sup>

Following the same procedure, two pseudomorphic samples featuring a Sn composition equal to 5 and 7 at. % (PS5 and PS7), respectively, were deposited by selecting a thicknesses well below the critical one for plastic relaxation.

X-ray measurements were performed using a 9 kW SmartLab diffractometer from Rigaku in high-resolution setup with a Ge(400)  $\times$  2 crystal collimator, a Ge(220)  $\times$  2 crystal analyzer, and  $\text{CuK}_{\alpha 1}$  radiation. For the *in situ* annealing experiments, a DHS1100 oven from Anton Paar was mounted on the diffractometer. The Bragg peak position of the symmetrical (004) diffraction of the Si substrate, Ge buffer layer, and GeSn layer was measured between room temperature (RT) and temperatures clearly above the occurrence of Sn segregation. The samples were heated in ambient  $\text{N}_2$  with 30 K/min, and at each individual measuring point, the sample stayed at a fixed temperature about 15–20 min: (i) about 5 min to check/correct the sample alignment on the Si(004) peak; (ii) about 10 min required to perform the  $\omega$ -2 $\Theta$  scans in the Si, Ge, and GeSn region.

The optical properties were studied using a micro-photoluminescence ( $\mu$ -PL, spot size of  $\sim 1 \mu\text{m}$ ) system equipped with a LN Linkam cryostat. As the excitation source, we used continuous-wave (cw) laser with the wavelength of 532 nm. The spectrometer (Horiba HR320) was equipped with a thermoelectric-cooled single-channel PbS detector (cut-off wavelength of  $\lambda \sim 3.2 \mu\text{m}$ ).

The sample crystal structure was investigated by (Scanning) transmission electron microscopy [(S)TEM] and energy-dispersive X-ray spectroscopy (EDX) using a FEI Tecnai Osiris instrument operated at 200 kV.

TABLE I. GeSn lattice parameters after different annealing processes (third column) determined by peak analysis at RT of the asymmetric GeSn (-2-24) reflection: thickness (d), out of plane ( $a_1$ ), in-plane ( $a_0$ ), and bulk ( $a_b$ ) lattice parameter, degree of relaxation (R) relative to the Ge buffer [reported only for  $T_A < T_C(x)$ ], Sn content (x), and in-plane strain ( $\epsilon_0$ ).

Sample	d (nm)	Annealing	$a_1$ (Å)	$a_0$ (Å)	$a_b$ (Å)	R (%)	x (%)	$\epsilon_0$ (%)		
REL5	770	(As-dep.)	5.7055	5.6926	5.6999	$78.7 \pm 1.5$	$4.8 \pm 0.1$	-0.130		
		Up to 700 °C	5.6583	5.6761	5.6659				$0.9 \pm 0.1$	+0.179
		30' at 350 °C	5.7036	5.6939	5.6995				$83.3 \pm 1.5$	$4.8 \pm 0.1$
PS5	54	(As-dep.)	5.7242	5.6661	5.6993	$1.3 \pm 1.5$	$4.8 \pm 0.1$	-0.582		
PS7	58	(As-dep.)	5.7560	5.6658	5.7173	$1.0 \pm 1.5$	$6.9 \pm 0.1$	-0.902		
REL9	420	(As-dep.)	5.7476	5.7162	5.7341	$73.7 \pm 1.5$	$8.8 \pm 0.1$	-0.312		
		Up to 500 °C	5.6616	5.6721	5.6661				$0.9 \pm 0.1$	+0.105
REL12	440	(As-dep.)	5.7804	5.7339	5.7605	$71.0 \pm 1.5$	$11.7 \pm 0.1$	-0.461		
		Up to 500 °C	5.6632	5.6718	5.6669				$1.0 \pm 0.1$	+0.086
REL12A		30' at 295 °C	5.7795	5.7329	5.7595	$71.8 \pm 1.5$	$11.6 \pm 0.1$	-0.462		

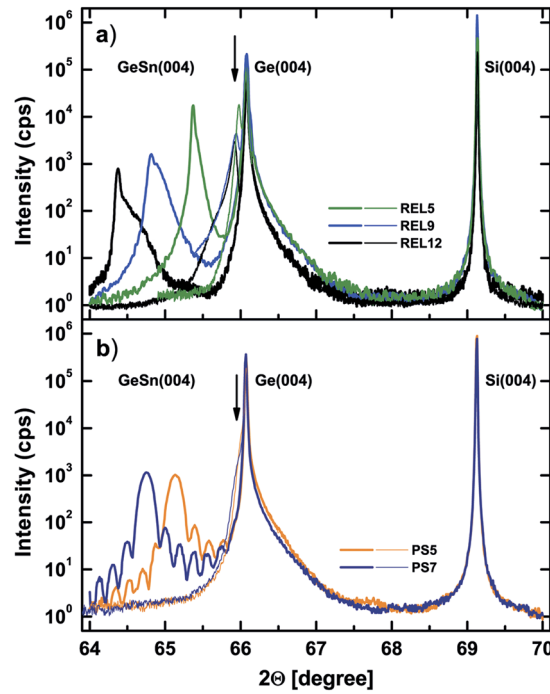


FIG. 1. Specular  $\omega$ - $2\theta$  scans of (004) diffraction for (a) all partially relaxed GeSn and (b) pseudomorphic GeSn samples measured at room temperature before (thick lines) and after (thin lines) high-temperature annealing treatment. The arrows mark the position of the GeSn (004) diffraction peak measured after high temperature treatment.

In Fig. 1, we present the specular  $\omega$ - $2\theta$  scans of the as-deposited (i.e., not annealed) GeSn/Ge/Si(001) samples featuring different Sn content and growth conditions (thick lines). The Si, Ge, and GeSn(004) peaks can be clearly distinguished both in the relaxed [REL, Fig. 1(a)] and in the pseudomorphic (PS, bottom panel) sample series. The pseudomorphically grown GeSn layers [Fig. 1(b)] show typical thickness fringes in the GeSn(004) peak. The slightly asymmetric shape of the Ge(004) peaks with increased intensity on the high-angle side is typical for the occurrence of interdiffusion at the Si/Ge interface during the preparation of the Ge/Si virtual substrates.<sup>15</sup> Similarly, the asymmetry of the GeSn(004) peak of partly relaxed samples indicates a variation of the Sn content over the layer depth, since Sn incorporation is slightly elevated after the onset of relaxation, as the larger lattice constant now allows for an increased number of Sn atoms to be built into the crystal.<sup>14</sup> The thin lines in Fig. 1 correspond to the  $\omega$ - $2\theta$  scans measured after thermal annealing at high temperature. In this case, as discussed in the following, the GeSn signal disappears both in relaxed and pseudomorphic samples. The  $\omega$ - $2\theta$  scans measured *in situ* during the heat treatment were fitted by multiple Gaussian profiles to determine the position ( $2\theta$  value), width, height, and area of the individual components. In the case of asymmetric Ge and GeSn peaks, the following analysis is using the data of the dominating component.

In Fig. 2(a), we display the  $T_A$ -driven evolution of the out-of-plane lattice parameter  $a_1$ , measured for the Si substrate, for the Ge buffer (for the REL5 sample only), and for the partly relaxed GeSn. As indicated by black arrows, the annealing cycle starts and ends at RT, reaching a sample-dependent critical temperature  $T_C(x)$  as the upper limit. At  $T_C(x)$ , the intensity of the initial  $\text{Ge}_{1-x}\text{Sn}_x(004)$  signal vanishes and, simultaneously, a new peak appears as a shoulder of the Ge(004) signal (vertical arrows in Fig. 1), pointing to a sudden Sn segregation and to the formation of a thermodynamically stable  $\text{Ge}_{0.99}\text{Sn}_{0.01}$  alloy with a smaller lattice constant.<sup>16</sup>

To support this statement, in Fig. 2(b), we show, as a function of  $T_A$ , the peak intensity of the GeSn(004) signals corresponding to the as-grown composition and to the new appearing  $x = 0.01$  phase. An abrupt transition from the high-Sn to low-Sn content phase occurs at a critical temperature  $T_C(x)$ , which decreases with the Sn content [see Fig. 2(c)]. Finally, we notice the decrease of the

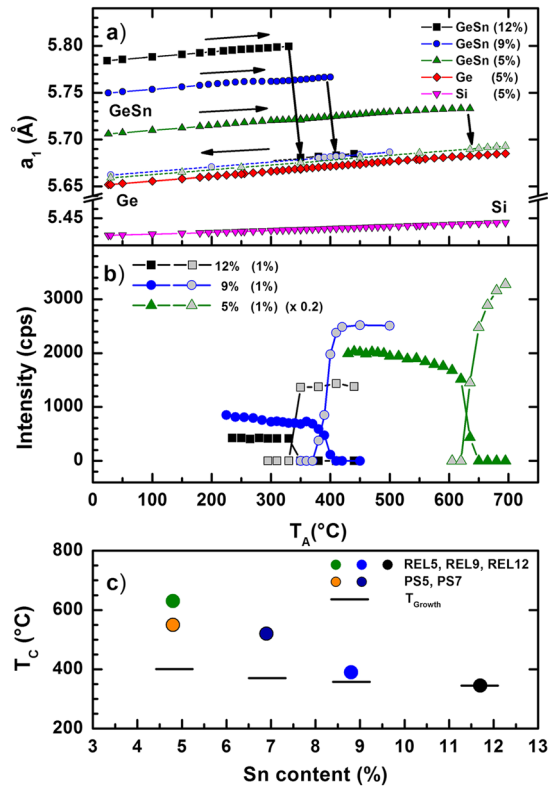


FIG. 2. (a) Out-of-plane lattice parameter  $a_1$  vs. annealing temperature measured for the main diffraction peaks of GeSn, Ge buffer, and the Si substrate for partially relaxed GeSn layers (REL5–12). Black arrows indicate the temperature cycling. (b) Peak height of the main two GeSn signals (see the text) in the temperature range of Sn segregation. Data acquired after reaching  $T_C(x)$  are plotted in panel (a) and (b) using gray filled symbols. (c) Sn segregation temperature  $T_C(x)$  vs. Sn content for relaxed and pseudomorphic samples. The growth temperature for each sample is displayed as black lines.

$\text{Ge}_{1-x}\text{Sn}_x(004)$  intensity observed when  $T_A$  approaches  $T_C(x)$ , associated with an increase of the diffraction peak width (not shown), which we attribute to the lattice disordering led by the increased  $T_A$  (Debye-Waller effect).

Accurate peak position measurements of the (004) and the asymmetrical (-2-24) reflections were performed at RT before and after the annealing cycle. This allows the simultaneous determination of the  $a_1$  and in-plane ( $a_0$ ) lattice parameters, from which we calculated the bulk lattice constant, the Sn content, and the degree of relaxation  $R$  (see Table I). This latter quantity is calculated as

$$R = (a_{0,\text{epi}} - a_{0,\text{Ge}}) / (a_{\text{bulk,epi}} - a_{0,\text{Ge}}) \times 100,$$

where  $a_{0,\text{epi}}$  and  $a_{\text{bulk,epi}}$  are the in-plane and bulk lattice parameter of the GeSn epi-layer, while  $a_{0,\text{Ge}}$  is the in-plane lattice parameter of the Ge buffer layer. To this aim, we notice that the Ge buffer layers of all samples show a slightly in-plane tensile strain of 0.13-0.15%, which is marginally modified after the heat treatment. In our analysis, we have used the linear interpolation between  $\alpha$ -Sn (6.49 Å) and Ge (5.657 Å) diamond lattice parameters.<sup>9</sup>

The composition values of the as-grown samples are in very good agreement with those measured by Rutherford backscattering spectrometry, witnessing the accuracy of the procedure used. All the three as-grown relaxed GeSn layers still show a residual heteroepitaxial compressive strain (i.e.,  $\epsilon_0 < 0$ ), corresponding to a strain relaxation in the 70% and 79% range. The plastic relaxation of those layers is accompanied by the formation of MDs at the Ge/GeSn interface, as clearly detected by TEM/STEM (see Fig. 3).

Moreover, when the annealing process occurs at  $T_A > T_C(x)$ , the epilayer, now in a segregated  $\text{Ge}_{0.99}\text{Sn}_{0.01}$  phase, shows a moderate tensile strain due to two different contributions. On one hand, the epilayer, interacting with the Si substrate via the Ge buffer, accumulates a residual tensile strain

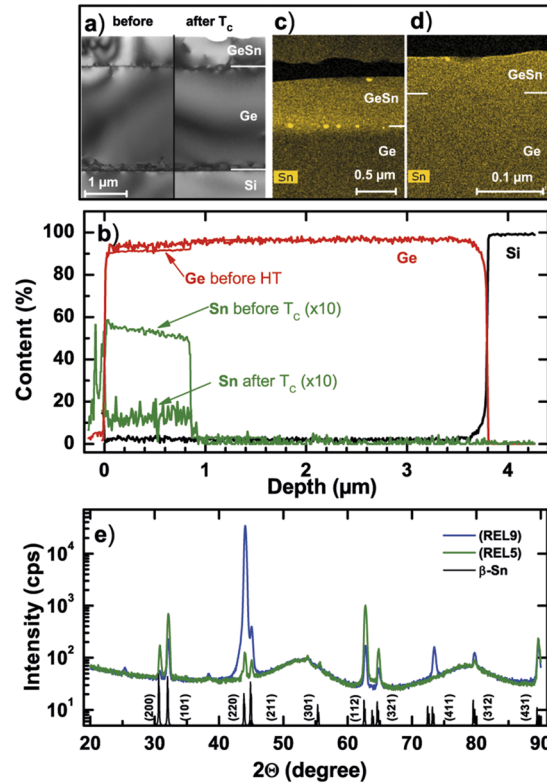


FIG. 3. (a) Cross sectional TEM micrographs of sample REL5 before and after high-temperature treatment; (b) EDX line scans before and after the annealing process (REL5); elemental EDX Sn distribution after annealing up to  $T_c$  for sample REL5 (c) showing Sn clusters both at the Ge/GeSn interface and at the surface and for sample PS5 (d) showing Sn clusters at the surface only; (e)  $2\theta$  scans in grazing incidence diffraction geometry with  $2^\circ$  angle of incidence measured on samples REL5 and REL9 after high-temperature annealing confirming the formation of  $\beta$ -Sn.

while cooling from the maximum annealing temperature (forming temperature) to RT, because of its bigger thermal expansion coefficient with respect to the Si substrate. Indeed, at  $x = 0.01$ ,  $a_{\text{bulk,epi}}$  is lower than the in-plane lattice parameter of the tensile strained Ge buffer. On the other hand, the MD network, already present before the annealing, “fixes” the in-plane lattice parameter of the epilayer regardless of its composition. Consequently, the shrinking of the lattice cell volume due to the decrease of the Sn content for  $T_A \geq T_C$  results in a tensile strain of the Sn-impoverished annealed epilayers.

In Fig. 3(a), we show the cross section TEM micrographs of sample REL5 before (left panel) and after (right panel) the complete annealing cycle up to  $T_C(x)$  and down to RT. After the thermal treatment, we observe the formation of Sn surface clusters, attributed to Sn out-diffusion. As already noticed, the Sn segregation leads to a lower effective Sn content in the bulk of the GeSn layer and consequently a decrease of the epitaxial strain, reversing its character from compressive to tensile<sup>17</sup> as indicated in Table I.

The EDX-measured elemental profile [Fig. 3(b)] indicates, in good agreement with the XRD results, that after the annealing treatment, the Sn content is reduced from 5 at. % to ~1 at. %, while the thickness of the GeSn layer is left unchanged. It is worth to notice in Fig. 3(b), for the as grown sample, the presence of a gradient of the Sn content, which matches well with the asymmetry of the GeSn XRD feature discussed when introducing Fig. 1. The EDX micrograph of the Sn distribution for sample REL5 after the annealing cycle [Fig. 3(c)] evidences the presence of Sn-rich clusters formed both at the surface (10-100 nm wide aggregates) and at the GeSn/Ge hetero-interface, most likely accumulating in the surrounding of the MD cores. In fact, the highly defected lattice close to the dislocation core, with its rather loose covalent bonds, enables the occupation of interstitial sites by Sn atoms, which can subsequently bind and form  $\beta$ -Sn defects.<sup>9</sup> Consequently, in the PS5

*pseudomorphic* sample [Fig. 3(d)], the Sn segregation is limited to the top sample surface only. XRD measurements in grazing incidence geometry confirm the existence of  $\beta$ -Sn crystallites with random orientation, as clearly see in Fig. 3(e), which we correlate to the Sn clusters observed at the surface. The weak peak observed at  $\sim 25^\circ$  in REL9 is compatible with the presence of few clusters made of ordered  $\text{Ge}_{0.5}\text{Sn}_{0.5}$  zinc blende structure with a 0.62 nm lattice parameter, most likely located within the epi-layer.<sup>11</sup>

Different from the report of Li *et al.*,<sup>6</sup> we do not observe, in samples of comparable Sn content and relaxation degree, Sn clustering in the bulk of the epi-layer. This might be due to the different growth technique (molecular beam epitaxy) and the rather low deposition temperature (160 °C) used in Ref. 6 that could have triggered a higher density of Ge vacancies in the epilayer. In fact, a high density of point defects could evolve in complex vacancy defects/clusters acting as seeds for the formation of non-substitutional segregated  $\beta$ -Sn defects,<sup>12</sup> as reported for a rather extreme case for the annealing of amorphous  $\text{Ge}_{0.92}\text{Sn}_{0.08}$  layers.<sup>18</sup>

To gain more insight on the annealing-driven plastic strain relaxation and segregation processes, in Fig. 4, we plot the change of  $a_1$  (relative to its value at room temperature) as a function of  $T_A$  for the three partially relaxed samples. Up to a temperature of  $\sim 260$ – $280$  °C, the relative change of  $a_1$

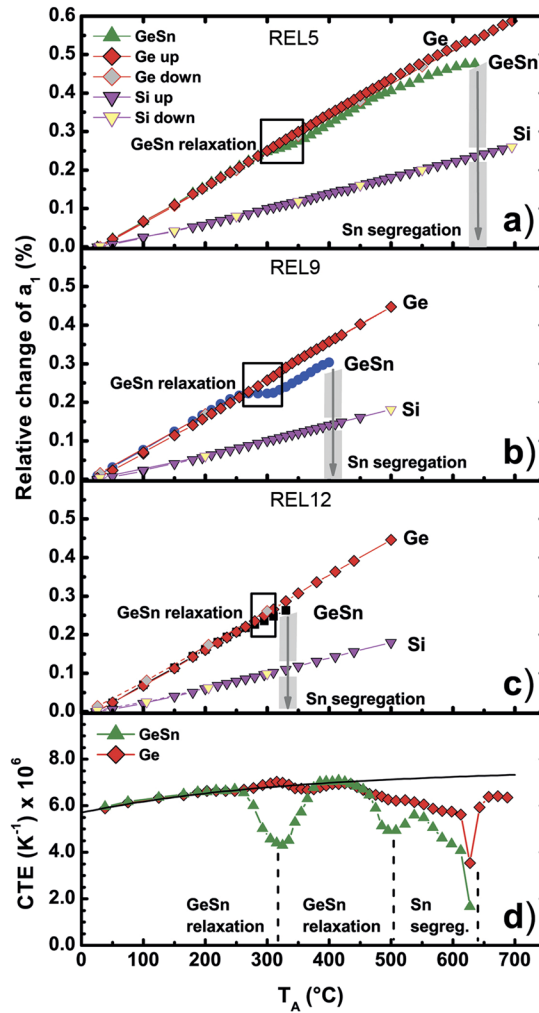


FIG. 4. [(a)–(c)] Relative change of out-of-plane lattice parameter  $a_1$  vs. temperature for all partly relaxed samples. As indicated in the legend, in panel (a), we indicate with different symbols the measurements acquired during the ramping-up or down to RT and gray arrows indicate the segregation  $T_C$ ; (d) estimated coefficient of thermal expansion (CTE) for the bulk lattice parameter of the GeSn and Ge buffer layer of sample REL5; the black line gives the CTE of Ge according to Ref. 19.

for GeSn and Ge is nearly constant, followed by a region (rectangles in Fig. 4) where the increase of  $a_1$  of the GeSn layer is smaller than that of Ge. In other words, we observe that, above an annealing temperature  $T_A = T_R$ , the GeSn out-of-plane lattice expansion abruptly “slows down.” This changing slope can be clearly seen by comparing the behavior of the coefficient of thermal expansion (CTE) of the GeSn and Ge layers. To this aim, the bulk lattice parameter of GeSn and Ge layers at RT was calculated from the measured  $a_1$  and  $a_0$  values (see Table I) using the same value of the Poisson ratio ( $\nu_{\text{Ge}} \sim 0.28$ ) for both materials, owing to the low Sn content. The temperature evolution of the lattice constant was estimated from the measured  $a_1$  values, assuming a T-independent constant relaxation R and Sn content x. A calculation of the bulk lattice parameter under these assumptions allows a correct evaluation of the GeSn CTE as long as no additional relaxation and/or segregation takes place. Indeed, it can be easily shown that if one or both of these processes occur, the CTE obtained with this procedure is underestimated. It follows that the thermal evolution of CTE can be used as a sensitive tool to probe the strain relaxation processes in a layer via, e.g., dislocation formation, segregation, or external influence by other layers.

In Fig. 4(d), we plot, as a function of  $T_A$ , the CTE of the GeSn and Ge buffer layer. The CTE of the GeSn layer shows clear deviations from the expected monotonic increase with temperature. This phenomenon could be attributed to: (i) a further lattice relaxation of the GeSn layer that decreases the tetragonal distortion of the lattice cell in the growth direction or (ii) the loss of volume of the lattice cell due to the beginning of the Sn segregation. Additionally, the CTE of Ge displays a difference to the value of bulk Ge according to Ref. 19 for  $T_A > 300$  °C. Since it was proven that the Ge buffer did not suffer further relaxation in the annealing process (see above), this indicates that the strain state of the Ge buffer is influenced by modifications in the GeSn layer above.

To individuate the main mechanism driving the observed behavior, the sample REL5, was annealed for 30 min at a temperature  $T_A = 350$  °C in the same experimental conditions as all the other samples investigated (named REL5A in Table I). After cooling down to RT, the layer parameters were determined by a precise peak analysis of the (004) and asymmetrical (-2-24) reflections. We observed no change of the Sn content within the experimental error, while the degree of relaxation increased by about 4%, corresponding to a decrease in the in-plane compressive strain from 0.13% to 0.098% (see Table I). We attribute the observed behavior to a further plastic relaxation of the strain in the GeSn film via the elongation of existing MD segments.

A similar behavior is observed in the case of the REL9 sample, where the strain relaxation increases from  $R = 74\%$  to  $79\%$  in the limited interval of temperature existing between the occurrence of the increased lattice relaxation and  $T_C$  ( $9\%$ )  $\sim 400$  °C, where the Sn segregation suddenly occurs [see Fig. 4(b)]. In sample REL12, this temperature range is negligible so that only a limited increased relaxation is allowed before the low Sn content phase formation [see Fig. 4(c)]. Nonetheless, here we point out that the annealing of the REL12 wafer at  $T_A = 295$  °C for 30 min ( $T_R < T_A < T_C$ , sample REL12A) did not induce any Sn segregation but only a weak extra relaxation (Table I).

By contrast, for sample REL5, a further gradual reduction of the increase of  $a_1$  above  $T \sim 500$  °C is observed [see Fig. 4(d)]. In agreement with the reports of Li *et al.*<sup>6</sup> and Comrie *et al.*,<sup>8</sup> we attribute this behavior to the beginning of the Sn out-diffusion, leading to the abrupt transition occurring at  $T_C$ . As pointed out before, in the higher Sn content samples, the transition to the thermodynamically stable  $\text{Ge}_{0.99}\text{Sn}_{0.01}$  phase occurs at lower temperatures and this gradual out-diffusion process cannot be observed.

We conclude thus that in *partially relaxed* GeSn epilayers, the annealing induces a further strain relaxation at temperature higher than  $T_R$ . The presence of TD and MD, linked to the plastic relaxation, enhances the Sn diffusion, at temperatures higher than (but relatively close to) that of plastic relaxation segregates forming  $\beta$ -Sn clusters. As a matter of fact, the Sn diffusivity in dislocated layers is enhanced by two-three orders of magnitude with respect to the bulk case,<sup>20</sup> occurring through the mono-vacancy diffusion dynamics.<sup>21</sup> The TD could then act as a preferential diffusion network, leading to the observed accumulation of Sn atoms and  $\beta$ -Sn defects at the heterointerface (see Fig. 3).

The results obtained on pseudomorphic samples support this interpretation. While REL5 shows, as discussed above, further relaxation at 300 °C and a rather fast segregation above 600 °C, the pseudomorphic sample does not show any relaxation before a relatively smooth segregation occurs

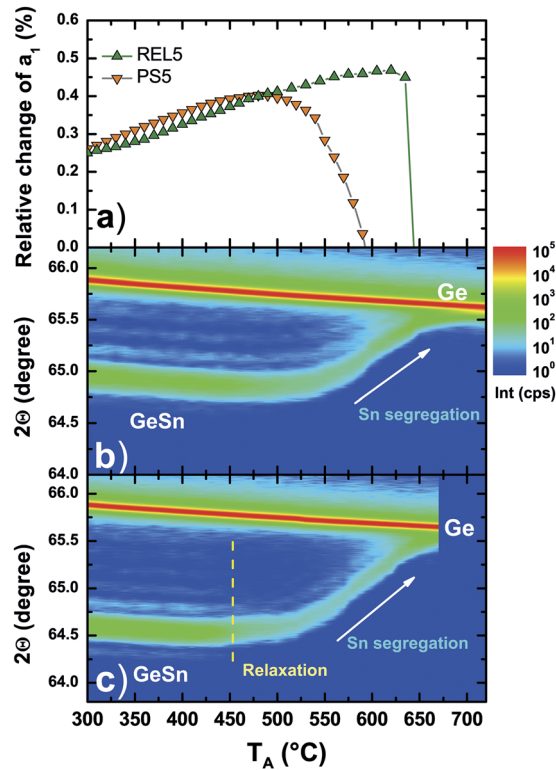


FIG. 5. (a) Comparison of the relative change of out-of-plane lattice parameter  $a_1$  vs. temperature between samples REL5 and PS5. 2D-plot of diffracted intensity vs.  $2\Theta$  and  $T_A$  for pseudomorphic GeSn samples PS5 (b) and PS7 (c).

[Fig. 5(a)]. This is confirmed in the 2D-plot of diffracted intensity vs.  $2\Theta$  and temperature in Fig. 5(b), where thickness fringes can be seen parallel to the GeSn signal until segregation starts. In fact, the existence of thickness fringes for heteroepitaxial structures is a sensitive indication for pseudomorphism, since they disappear after a few percent of relaxation, owing to the “blurring” of the lattice at the heterointerface due to the MDs.<sup>22</sup> Sample PS7 shows the same smooth segregation [Fig. 5(c)], but different to PS5 relaxation starts at  $\sim 450$  °C, which is clearly indicated by the disappearance of the thickness fringes.

The XRD analysis results are complemented by  $\mu$ -PL data. In Fig. 6(a), we compare the PL spectra of REL5 and its annealed twin sample REL5A, acquired at 80 K. Both samples are slightly indirect semiconductors whose PL spectrum is dominated by two emission features that we attribute to the  $\Gamma$ -HH (higher energy) and L-HH (lower) recombination, respectively.<sup>23</sup> In the annealed sample REL5A, we observe that the spectral weight of the  $\Gamma$ -HH transition is more pronounced and red-shifted and the PL spectral width is reduced from  $\sim 82$  meV to 67 meV. These observations cope well with the increased plastic relaxation induced by the annealing discussed above.<sup>24</sup> In fact, the observed increased intensity and line narrowing can be attributed to both the “more direct” nature of the band structure triggered by a smaller compressive strain and the increase of the non-radiative recombination time brought about by the beneficial effect of the annealing process on the crystal quality. It is interesting to notice that in the REL12 sample (Fig. 6), a similar comparison with its annealed counterpart REL12A only shows a narrowing and an increase in intensity of the emission line, while the spectral shift is negligible. This observation is in agreement with the XRD data for REL12 and REL12A that indicate a marginal strain relaxation upon annealing.

In summary, we have investigated the impact of the annealing process on plastically relaxed and pseudomorphic CVD grown GeSn epi-layers. Pseudomorphic epi-layers do not show any plastic relaxation before the occurrence of the segregation process that *progressively* leads to the accumulation of Sn at the surface and to the formation of an equilibrium stable  $\text{Ge}_{0.99}\text{Sn}_{0.01}$  alloy. The annealing of GeSn layers with pre-existing dislocations results initially in a further plastic

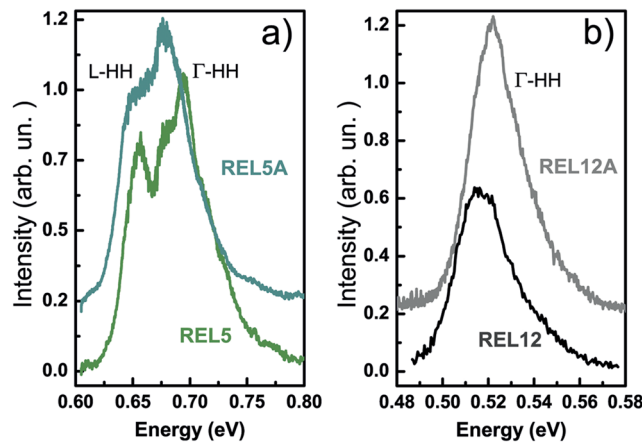


FIG. 6. Photoluminescence spectra taken at 80 K for samples (a) REL5 (as-grown) and REL5A (after annealing at 350 °C for 30 min) and (b) REL12 (as-grown) and REL12A (after annealing at 295 °C for 30 min). In each panel, we have offset the two spectra for clarity.

relaxation of the heteroepitaxial strain followed by a *sudden* Sn segregation. The Sn segregation temperature decreases, almost linearly, with the Sn content. These results point to the relevant role of extended defects existing in the partially relaxed layer in enhancing the Sn diffusion.

Our results shed light on the possibility to modify the strain state of a GeSn layer by appropriate thermal treatment processes, while avoiding Sn segregation. The strength of this effect strongly depends on the growth temperature, elastic lattice strain, and layer stoichiometry. Generally, annealing at a temperature below the occurrence of Sn segregation allows an improvement of layer quality, as reflected in the improved optical quality of the material.

The authors acknowledge financial support by the BMBF in frame of the M-ERA.NET project GESNAPHOTO and support by the German Research Foundation (DFG) through the project “SiGeSn Laser for Silicon Photonics.”

- <sup>1</sup> C. Kopp, S. Bernabé, B. B. Bakir, J. M. Fedeli, R. Orobtaouchouk, F. Shrank, H. Porte, L. Zimmermann, and T. Tekin, *IEEE J. Sel. Topics Quantum Electron.* **17**, 498 (2011).
- <sup>2</sup> S. Wirths, R. Geiger, N. von den Driesch, G. Mussler, T. Stoica, S. Mantl, Z. Ikonić, M. Luysberg, S. Chiussi, J.-M. Hartmann, H. Sigg, J. Faist, D. Buca, and D. Grützmacher, *Nat. Photonics* **9**, 88 (2015).
- <sup>3</sup> S. Al-Kabi, S. A. Ghetmiri, J. Margetis, T. Pham, Y. Zhou, B. W. D. Collier, R. Quinde, W. Du, A. Mosleh, J. Liu, G. Sun, R. A. Soref, J. Tolle, B. Li, M. Mortazavi, H. A. Naseem, and S.-Q. Yu, *Appl. Phys. Lett.* **109**, 171105 (2016).
- <sup>4</sup> V. Reboud, A. Gassenq, N. Pauc, J. Aubin, L. Milord, Q. M. Thai, M. Bertrand, K. Guillois, D. Rouchon, J. Rothman, T. Zabel, F. Armand Pilon, H. Sigg, A. Chelnokov, J. M. Hartmann, and V. Calvo, *Appl. Phys. Lett.* **111**, 092101 (2017).
- <sup>5</sup> J. Margetis, S. Al-Kabi, W. Du, W. Dou, Y. Zhou, T. Pham, P. Grant, S. Ghetmiri, A. Mosleh, B. Li, J. Liu, G. Sun, R. Soref, J. Tolle, M. Mortazavi, and S.-Q. Yu, *ACS Photonics* **5**(3), 827–833 (2018).
- <sup>6</sup> H. Li, Y. X. Cui, K. Y. Wu, W. K. Tseng, H. H. Cheng, and H. Chen, *Appl. Phys. Lett.* **102**, 251907 (2013).
- <sup>7</sup> R. Chen, Y.-C. Huang, S. Gupta, A. C. Lin, E. Sanchez, Y. Kim, K. C. Saraswat, T. I. Kamins, and J. S. Harris, *J. Cryst. Growth* **365**, 29 (2013).
- <sup>8</sup> C. Comrie, C. B. Mtskli, P. T. Sechogela, N. M. Santos, K. van Stiphout, R. Loo, W. Vandervorst, and A. Vantomme, *J. Appl. Phys.* **120**, 145303 (2016).
- <sup>9</sup> F. Gencarelli, D. Grandjean, Y. Shimura, B. Vincent, D. Banerjee, A. Vantomme, W. Vandervorst, R. Loo, M. Heyns, and K. Temst, *J. Appl. Phys.* **117**, 095702 (2015).
- <sup>10</sup> Y. Han, Y. Song, X. Chen, Z. Zhang, J. Liu, Y. Li, Z. Zhu, H. Huang, J. Shao, and S. Wang, *Mater. Res. Express* **5**, 035901 (2018).
- <sup>11</sup> A. A. Tonkikh, N. D. Zakharov, A. A. Suvorova, C. Eischmidt, J. Schilling, and P. Werner, *Cryst. Growth Des.* **14**, 1617 (2014).
- <sup>12</sup> J. D. Fuhr, C. I. Ventura, and R. A. Barrio, *J. Appl. Phys.* **114**, 193508 (2013).
- <sup>13</sup> J. M. Hartmann, A. Abbadie, N. Cherkashin, H. Grampeix, and L. Clavelier, *Semicond. Sci. Technol.* **24**, 055002 (2009).
- <sup>14</sup> N. von den Driesch, D. Stange, S. Wirths, G. Mussler, B. Holländer, Z. Ikonic, J. M. Hartmann, T. Stoica, S. Mantl, D. Grützmacher, and D. Buca, *Chem. Mater.* **27**, 4693 (2015).
- <sup>15</sup> K. H. Lee, S. Bao, B. Wang, C. Wang, S. F. Yoon, J. Michel, E. A. Fitzgerald, and C. S. Tan, *AIP Adv.* **6**, 025028 (2016).
- <sup>16</sup> S. Wirths, D. Buca, and S. Mantl, *Prog. Cryst. Growth Charact. Mater.* **62**, 1 (2015).
- <sup>17</sup> C. Fleischmann, R. R. Lieten, P. Hönicke, B. Beckhoff, F. Seidel, O. Richard, H. Bender, Y. Shimura, S. Zaima, N. Uchida, K. Temst, W. Vandervorst, and A. Vantomme, *J. Appl. Phys.* **120**, 085309 (2016).
- <sup>18</sup> R. Takase, M. Ishimaru, N. Uchida, T. Maeda, K. Sato, R. R. Lieten, and J. P. Locquet, *J. Appl. Phys.* **120**, 245304 (2016).

- <sup>19</sup> G. Capellini, M. De Seta, P. Zaumseil, G. Kozlowski, and T. Schroeder, *J. Appl. Phys.* **111**, 073518 (2012).
- <sup>20</sup> É. V. Dobrokhotov, *Phys. Solid State* **47**, 2257 (2005).
- <sup>21</sup> M. Friesel, U. Södervall, and W. Gust, *J. Appl. Phys.* **78**, 5351 (1995).
- <sup>22</sup> G. Bhagavannarayana and P. Zaumseil, *J. Appl. Phys.* **82**, 1172 (1997).
- <sup>23</sup> D. Stange, S. Wirths, N. von den Driesch, G. Mussler, T. Stoica, Z. Ikonc, J. M. Hartmann, S. Mantl, D. Grutzmacher, and D. Buca, *ACS Photonics* **2**, 1539 (2015).
- <sup>24</sup> S. Gupta, B. Magyari-Köpe, Y. Nishi, and K. C. Saraswat, *J. Appl. Phys.* **113**, 073707 (2013).